Tailoring block copolymer nanoporous thin films with acetic acid as a small guest molecule.

Alberto Alvarez-Fernandez[*a,b], *Fernando Valdes-Vango*[c,d], *José Ignacio Martín*[c,d], *María Vélez*[c,d], *Carlos Quirós*[c,d], *Daniel Hermida-Merino*[e], *Giuseppe Portale*[f], *José María Alameda*[c,d] *and Francisco Javier García Alonso*[a,d].

[a.] Dpto. Quimica Orgánica e Inorgánica, Universidad de Oviedo, 33006 Oviedo, Spain.

[b.] Department of Chemical Engineering, University College London, Torrington Place, London WC1E 7JE, UK.

[c.] Dpto. Física, Universidad de Oviedo, 33007 Oviedo, Spain

[d.] CINN (CSIC-Universidad de Oviedo), 33940, El Entrego, Spain

[e.] Netherlands Organization for Scientific Research (N.W.O.), DUBBLE CRG@ESRF, Grenoble 38042, France

[f.] Macromolecular Chemistry and New Polymeric Material, Zernike Institute for Advanced Materials, University of Groningen, Nijenborgh 4, 9747 AG, Groningen, The Netherlands

Email: alberto.fernandez@ucl.ac.uk

Abstract

Block copolymers offer the fabrication of mesoporous thin films with distinct nanoscale structural features. In this contribution, we present the use of acetic acid (CH_3COOH) as a low molecular weight guest molecule to tune the supramolecular assembly (SMA) of poly(styrene-block-4-vinylpyridine) (PS-*b*-P4VP), offering a versatile and straightforward method to obtain tailored nanostructured films with controlled topography and pore size. Spin-coating toluene solutions of PS-*b*-P4VP, with a variable amount of CH_3COOH, leads to micellar thin films, where the micelles contain the carboxylic acid as a guest molecule. The size can be conveniently modified in these films (from 48 to 75 nm) by varying the amount of organic acid in the starting solutions. Subsequent surface reconstruction of micellar films using ethanol (EtOH), led to ring-shaped copolymer nanoporous films with modulated diameter. Controling the micelle reconstruction process, cylindrical porous films are also obtained. Interestingly, changing the type of aliphatic carboxylic acids led to a modification of the observed film morphology from micelles to out-of-plane P4VP cylinders (or lamellae) in a PS matrix.

Introduction

Porous polymer films have been revealed as promising candidates for a wide range of applications, such as gas and energy storage[1], separation and purification membranes[2], sensor applications[3] or optical coatings[4]. While a great number of methods have been described to prepare them[5], the fabrication of nanoporous films with tailored and uniform pore size and shapes remains as a challenge[6–8].

BCP self-assembly is a well-known approach to create ordered nanoscale structures with tuneable size and morphology through control over a small number of key parameters, such as the relative volume fraction of the blocks (φ), the degree of polymerization (N), the Flory-Huggins parameter (χ_{ab}) and the deposition conditions[9,10]. Different strategies have been developed to create ordered mesoporous films using BCP self-assembly, generally including minor BCP domain removal by harsh chemical procedures[11,12]. On the other hand, the pores can also be obtained following a mild method, called reconstruction process, based on physical changes and excluding any chemical reactivity. First, the spin-coated (micellar or cylindrical) films are immersed in a selective solvent. Subsequently, the copolymer block located either in the micelle nucleus or in the cylinder swells with the solvent, migrating onto the film surface. Second, after evaporation of the solvent, the swelled chains shrink creating the observed pores[13].

Ring shaped BCP thin films constitutes a non-native structure in diblock copolymer bulk systems, even if toroidal micelles have been synthesized in solution[14,15]. Ordered ring shaped porous films have attracted particular interest due to their unique geometry and potential utility in materials fabrication[16–18]. Several routes have been explored to obtain this unusual morphology: most

notably by expanding and contracting different BCP domains in the self-assembled film[19] or by treating micellar films with acidic or basic water solutions[17,20,21].

The supramolecular assembly (SMA) of BCPs, where small molecules (SM) are covalently or non-covalently bonded to one of the blocks, constitutes an interesting strategy that has been extensively studied in recent years for the tuning of BCP thin film morphologies. Indeed, a number of SM-induced order to order transitions have been observed[22–24]. In other cases, this method has been applied to tune the obtained feature size, either by the SM to BCP ratio[25] or by shifting to a different SM during the process[26].

When designing a materials route with morphologies ranging from cylindrical to ring shaped BCP porous films, two processes need to be optimized. First, the fabrication of a homogeneous initial BCP micellar film with controllable diameter, and second, the micelle inversion process that leads to the final pore geometry. It is thus be of high value to select a single small molecule that can be used to adjust simultaneously both processes involved.

Aliphatic carboxylic acids have been largely employed with different PS-PVP copolymers, in solution, to obtain micelles or hollow vesicles[27] or polymers porous films[28] as a result of the R-COOH ability to form H-bonds with the pyridine ring. They represent a versatile SM since they are miscible with commonly used organic solvents i.e. toluene or ethanol and more importantly, enable to alter the pH environment of the micelle cores.

In this work, it has developed a novel approach in mild conditions to generate from BCP micellar to ring shaped porous films in a straightforward way. Particularly, acetic acid (CH_3COOH) has been used as an extractable small guest-molecule for the fabrication of nanostructured PS-*b*-P4VP copolymer films. Toluene solutions of a single PS-*b*-P4VP BCP, containing CH_3COOH, afford us

to fine-tailor firstly the micelle size and, after the subsequent reconstruction process, the morphology and pore size of the porous films. They were obtained by simply modifying the ratio between the SM and P4VP block, without adding homopolymers[29] or changing the BCP molecular weight. Other aliphatic carboxylic acids i.e. formic acid (HCOOH) and propionic acid have been also used to tune the morphology of the initial BCP film from micelles to cylinders and lamellae, showing the great versatility of this approach.

Experimental

Materials

PS-*b*-P4VP diblock copolymer, with M_n (PS)=47.0 kg mol^{-1} and M_n (P4VP)=25.0 kg mol^{-1}, was purchased from Polymer Source Inc. and used as received. Based on the volume fraction of each block, an hexagonal arrangement of P4VP cylinders in a PS matrix is expected[30,31]. CH_3COOH (glacial, 99-100%), HCOOH (puriss, ≥98%), propionic acid (≥99%) toluene (dry, 99.8%) and EtOH (absolute, 99.5%) were purchased from Sigma-Aldrich, and used without further purification. Silicon wafers (1 0 0) were purchased from CrysTec GmbH and cut to appropriate dimensions (approximately 1 × 1 cm^2). Silicon substrates were successively cleaned in acetone and Milli-Q water in an ultrasonic bath, and dried under nitrogen flow. Silicon nitride membranes of 50 nm in thickness prepared for TEM measurements were purchased from Agar Scientific.

Sample preparation

Solution preparation: The starting BCP solutions were prepared as follows. The appropriate amount of PS-*b*-P4VP and the required quantity of CH_3COOH (same for the other SMs) for the desired CH_3COOH:P4VP molar ratios were dissolved in dry toluene and stirred overnight in closed vials on a heating plate at ca. 70 °C and finally filtered through 0.45 μm filters (VWR). This filtration step is necessary to remove any dust or big particles present in the solution that could perturb the self-assembly during the spin-coating process, but the filter pores are enough big to do not have any impact in the CH_3COOH:P4VP ratio.

Film deposition: The BCP solutions were spin-coated at 2000 rpm rotational speed and at 1000 rpm s^{-1} rotational acceleration for 60s, using a Spinner SPIN 150 (SPS, Holland), onto silicon wafers or silicon nitride substrates. The thickness of the obtained films was measured in reflectance using a Filmetrics F20 instrument.

Surface reconstruction: In a subsequent process, the films were immersed in EtOH in a close vial for one hour to prepare the ring shaped nanoporous films or in CH_3COOH for 15 min to obtain the cilindrical porous films. In both cases, the films were then dried under nitrogen flow.

Atomic Force Microscopy (AFM)

Topography AFM images were obtained in contact mode using a scanning probe microscope controlled by a Nanotec controller (Nanotec SL), operated under an ambient atmosphere. Si_3N_4 tips with 15nm radius and enhanced reflectivity through Au/Cr coating were purchased from Olympus. Average micellar diameters were obtained from analysis of real space topography images using the 'flooding' tool of WSxM software[32]

Infrared (IR) spectra

IR spectra were recorded with a PerkinElmer Paragon 1000 FT-IR spectrometer.

Transmission Electron Microscopy (TEM)

TEM images were obtained with a MET JEOL-2000 EX-II on reconstructed films deposited on Si_3N_4 TEM membranes and consecutively tinctured through exposure to I_2 vapors in a closed vessel for 24h, due to its affinity to pyridine domains.

Dynamic light scattering (DLS)

Size distributions of the PS-b-P4VP (0.3 wt. %) toluene solutions, with various CH_3COOH:P4VP ratios (0:1; 1:1 and 10:1), were measured with a Malvern High Performance Particle Sizer. Each measurement was run five times.

Grazing Incidence Small Angle X-ray Scattering (GISAXS)

GISAXS experiments were performed on the Dutch Belgian Beamline at the European Synchrotron Radiation Facility(ESRF) station BM26B in Grenoble[33–35]. The beam illuminates the samples with a typical footprint of 150 mm^2. 2D scattering patterns were collected with a PILATUS 1MDectris detector and the sample-to-detector distance was set to 7000 mm. The beam center position and the angular range were calibrated using a silver behenate standard sample. The wavelength of the X-ray photons was 0.154 nm. Images have been recorded at an incident angle of 0.16° close to the critical angle of the block-copolymer thin film (α_c^{P4VP} = 0.165° and α_c^{PS}=

0.155°) to maximize the scattered intensity from the thin film. Corrections for the incoming beam intensity and the air background were applied before calculating the GISAXS intensity cuts.

Results and discussion

Control of micelle size with CH_3COOH:P4VP ratio. Toluene solutions of PS-b-P4VP (0.3 wt. %), with different CH_3COOH:P4VP ratios were spin-coated onto cleaned silicon substrates. As toluene is a good solvent for PS, but non-solvent for P4VP, spherical micellar structures are formed with PS shell and P4VP corona[36,37]. Fig. 1 shows the topographical AFM micrographs of the obtained nanostructured films (41 nm thick). In previous works, host molecule should be changed in order to obtain micelles with different size[38,39]. In contrast, in our case, the diameter of the micelles in the obtained film grew regularly with increasing CH_3COOH:P4VP ratio in the initial copolymer solution. While the pristine BCP micelles were sized at 46 ± 2 nm the micelle diameter increased to 63±1.7 nm for a 1:1 ratio. Finally, with a 10:1 CH_3COOH:P4VP ratio, the micellar diameter reached 75 ± 1.5 nm, constituting an increase of 63% on the initial micelle size. Average micellar diameters were obtained from analysis of real space topography images using the 'flooding' tool of WSxM software[32] (see Fig. S1). Interestingly, DLS measurements of the solutions show also a gradual increase of the micellar diameter related to the gradual increase of the CH_3COOH:P4VP ratios in the solutions, confirming the interaction between the carboxylic acid and the BCP (Fig S2).

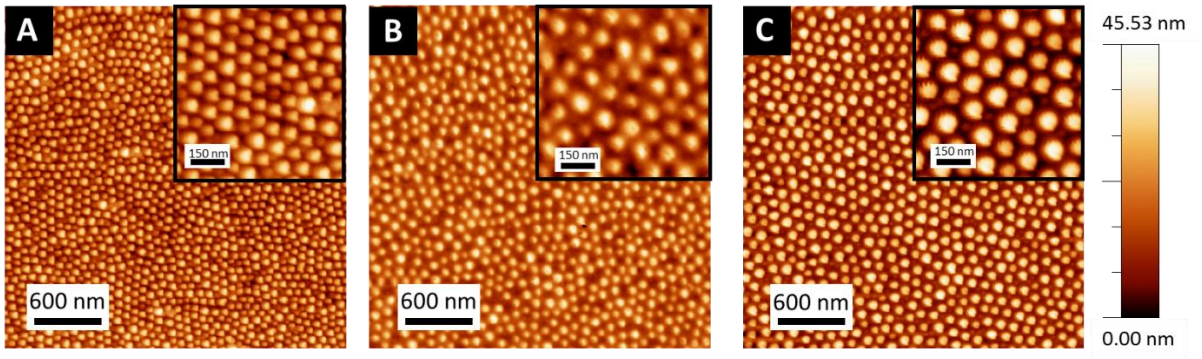

Figure 1: AFM topographical micrographs of as spun-coated micelles obtained from toluene solutions of PS-b-P4VP (0.3 wt. %) at different CH_3COOH:P4VP ratios: A) 0:1, B) 1:1, C) 10:1

In order to elucidate the nature of the interaction between the CH_3COOH molecules and the polymer pyridine rings, IR spectroscopy was implemented. Fig 2 shows the IR spectra obtained after evaporating several drops of PS-b-P4VP (0.3 wt. %) with different CH_3COOH:P4VP ratios onto a KBr disk for 12h in vacuum. The shift of the free pyridine bands at 993 and 1415 cm^{-1} for the copolymer (Fig. 2A) to about 1012 and 1418 cm^{-1} respectively when the acetic acid is added (Fig. 2B and 2C) clearly indicates H-bonding formation[39,40]. In addition, the gradual shift of the aromatic band of the free pyridine in P4VP from 1597 cm^{-1} (Fig. 2A) to 1600 cm^{-1} (Fig. 2B) and to 1603 cm^{-1} (Fig. 2C) with an increase in CH_3COOH:P4VP ratio, reflects an increased number of acid molecules hydrogen bonded to the copolymer macromolecules. An additional evidence of Py…H-OOCR bonding (see Fig. S3) is provided by the broad band at 2580 cm-1, which is a characteristic of a hydrogen bond carboxylic acid−pyridine[41,42]. The IR also shows the typical bands of the acetic acid at 1714 cm^{-1} and 1270 cm^{-1}.

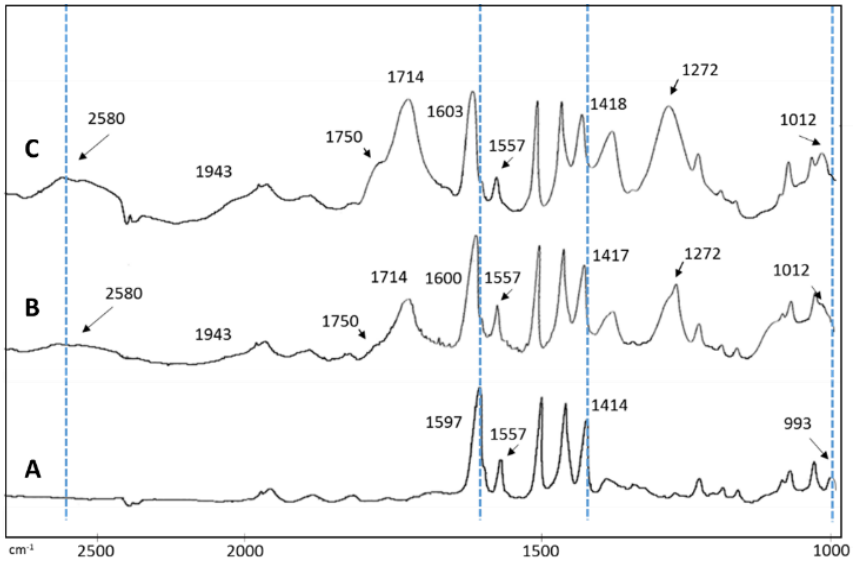

Figure 2: Infrared spectra (from 3000 to 900 cm-1) of samples obtained evaporating in vacuum toluene solutions of PS-b-P4VP (0.3 wt. %), at different CH_3COOH:P4VP ratios: A) 0:1, B) 1:1 and C) 10:1.

There is not any evidence supporting the existence of a pyridinium ion produced as a consequence of a hypothetical net proton transfer from the acetic acid to the pyridine fragment (see Fig. S3). The absence of a band around 1637 cm^{-1}, corresponding to the pyridinium ion[43] and the persistence of the weak band a 1557 cm^{-1}, which disappears when the pyridine ring is protonated[43], clearly demonstrate the inexistence of Py-H^+ cations. Therefore, IR spectra provide a clear proof of the presence of acetic acid H-bonded to the pyridine micelle cores, i.e. of the role of acetic acid as host molecule in the micelles.

Surface reconstruction of micellar films

Formation of ring-shaped copolymer films by surface reconstruction

Fig. 3A-B shows the topographical AFM micrographs of the nano-rings obtained from the PS-b-P4VP micellar films with CH_3COOH:P4VP ratios of 1:1 and 10:1 respectively. It has been found a size dependence of the diameter of the ring shaped nanoporous generated from the corresponding micellar film following the reconstruction procedure. Nano-rings obtained from the smaller micelles, (Fig. 3A), have lower radius, 75±2.1 nm, than those prepared from bigger micelles, 98±1.7 nm, (Fig. 3B) the greater the micelle the bigger the ring originated from it.

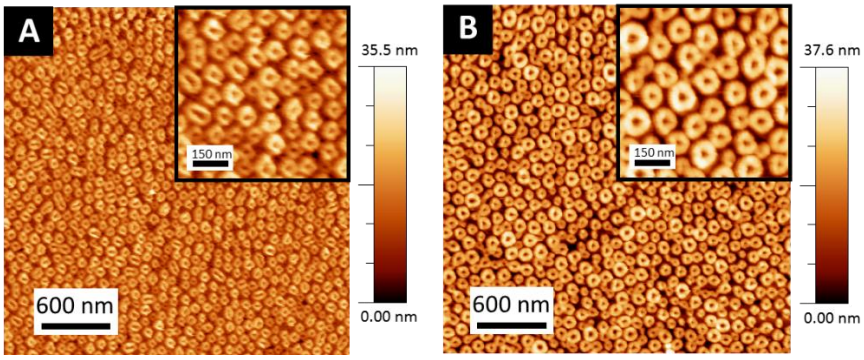

Figure 3: AFM topographical micrographs of ring-shaped PS-b-P4VP (0.3 wt. %) films with different CH_3COOH:P4VP ratios: A) 1:1, B) 10:1, obtained after a reconstruction in EtOH for 1h.

The ability of control the ring size is particular important, since it is a rare and broadly applicable morphology in diblock copolymer systems[44]. The possibility of not only obtaining but rather having a precise control of the structural parameters is an interesting step forward[16,45]. The ring-shaped morphology was confirmed by TEM (Fig. S4A). In transmission mode a clear array of dark rings with clear cores was observed, pointing out that no pyridine is inside the ring. This indicates a full inversion of the P4VP-core/PS-corona micellar nanostructure during the surface

reconstruction process: the P4VP core has transformed into a small ring with a nanopore at its centre (topographical profiles of all the samples are presented in Fig S5). Separately, FT-IR spectroscopy confirms that all the acetic acid contained in the micelles has been completely extracted after 1 hour in ethanol. Thus, the IR spectrum of a sample obtained evaporating a solution of PS-b-P4VP (0.3 wt. %), with a 10:1 CH_3COOH:P4VP ratio is identical to curve A in Fig. 2, corresponding to a pure PS-b-P4VP solution with no acetic acid (Fig. S6).

Previous works have shown the importance of the pH control during the BCP reconstruction process[21,45,46]. In our case, the presence in the solution of the CH_3COOH molecules that were extracted from the micelle cores caused a change in the acidity of the solution that was found to be essential for the ring shape formation. Fig. S4B shows the porous film obtained following the same reconstruction procedure than in the previous cases but with BCP pristine micelles. No ring-shaped features are obtained but a hexagonal distribution of cylindrical pores in a PS matrix, confirming the essential role of the CH_3COOH molecules during the ring-shape formation. Other parameters that have been revealed important in the formation of the ring features and that can be controlled with the presence of the SM is the size and the inter-distance of the micelles in the film[17].

Film morphology characterization by Grazing Angle Small Angle-Scattering (GISAXS)

Film morphology modifications by the reconstruction process were further confirmed by GISAXS measurement. GISAXS constitute a powerful tool to analyse BCP film morphology[47,48] on a larger scale than AFM and TEM. Two identical films were obtained by spin-coating of a PS-b-P4VP toluene solution (0.3 wt. %), with a 10:1 CH_3COOH:P4VP ratio at 3000 rpm and 1500 rpm^2, generating micellar films. Then, one of them was immersed for 1 hour in EtOH in order to prepare

a reconstructed nanoring film. Fig. 4 shows the results of the GISAXS measurements for these micellar (Fig. 4A) and reconstructed nanoring films (Fig. 4B). 2D GISAXS scattered intensity in the α_f vs. 2θ plane (where α_f is the exit angle in the out-of-plane vertical direction and 2θ is the scattering angle in the in-plane horizontal direction) present strong lobes symmetrically located at both sides of the specular scattering plane, indicative of the typical sizes and spatial arrangement of the nanostructured copolymer morphology.

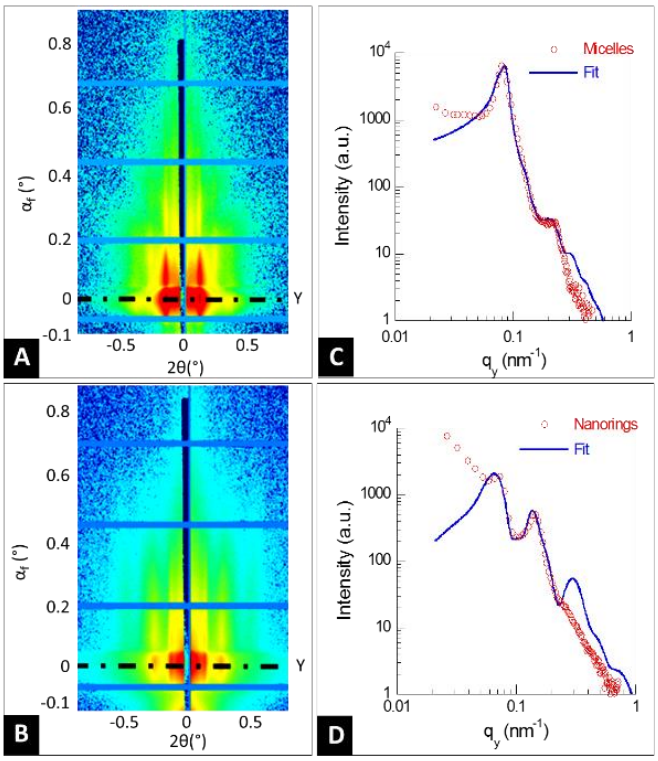

Figure 4 GISAXS intensity patterns in the α_f vs. 2θ plane for (A) micellar film and (B) nanoring film. The dashed line corresponds to the Yoneda peak (Y). Angles are measured in degrees along both axes. GISAXS intensity cuts at the Yoneda peak along q_y for (C) micelles and (D) nanorings. Blue lines are the best fit obtained using a distorted hexagonal packing of (C) P4VP spheres and (D) P4VP hollow cylinders in a PS matrix.

Inspection of the 2D GISAXS patterns shows a clear change of morphology as well as dimensions of the reconstructed film. The typical GISAXS 2D pattern for a layer of spherical objects deposited on a surface was found for micellar films (see Fig 4A). The position $q^* = 0.0798$ nm^{-1} of the first Bragg peak indicates a period of $L_0 = 2\pi/q^* = 78.73$ nm between scattering planes. Higher order Bragg rods are observed at $q_y/q_y^* = \sqrt{3}$, confirming the hexagonal ordering of the BCP structure (clearly observed also in the AFM images). The GISAXS 2D pattern of the ring-shaped porous film indicated the presence of core-shell objects and confirming the successful reconstruction of the micellar films.

In order to obtain further quantitative information on the film morphology, GISAXS intensity cuts (1D profile) have been calculated at the Yoneda peak position, i.e. when α_f is equal to the critical angle of the system, along the horizontal wavevector q_y, (see Fig. 4). q_y is defined as $q_y = k_0 [\sin(2\theta) \cos(\alpha_f)]$ where $k_0 = 2\pi / \lambda$ and $\lambda = 0.155$ nm, the X-ray wavelength. The 1D profiles reveal the presence of several satellite peaks related to the local order of the copolymer films and can be analysed using different models[49] in order to obtain details about the nanostructured block-copolymer films. Best fit of the micellar film scattering intensity (see Fig. 4C, solid line) is obtained for a model of spherical P4VP domains with average diameter 64 nm, forming a distorted hexagonal lattice with intermicellar distance 96 nm. However, the best fit of the intensity profile (1D plot) of the reconstructed film (see Figure 4D), was obtained using a model of an hexagonal assembly of P4VP hollow cylinders in a PS matrix with lattice constant 110 nm, confirming the nanoring morphology observed by AFM. This model allow us to extract the two more important parameters in order to characterize the ring structure, the internal and the external diameter of the rings (see Fig S7). The calculated thickness of the P4VP rings was about 35 nm and the internal hole diameter was about 16 nm, so that nanoring diameter was 85 nm.

From nano-rings to cylindrical porous surfaces with controllable pore size.

Fig. 5 shows the topographical AFM images of the porous films obtained from the PS-b-P4VP micellar films with CH_3COOH:P4VP ratios of 1:1 and 10:1 respectively, after be immersed in a pure CH_3COOH solution for 15 min. As mentioned earlier, the pH of the medium during the reconstruction process plays an important role in the obtained pore morphology. Interestingly, cylindrical porous surfaces were obtained when the reconstruction process was carried out in pure acetic acid solution. As in the case of the nano-ring films, the presence of the CH_3COOH molecule in the core of the starting micellar film allows to control the pore size.

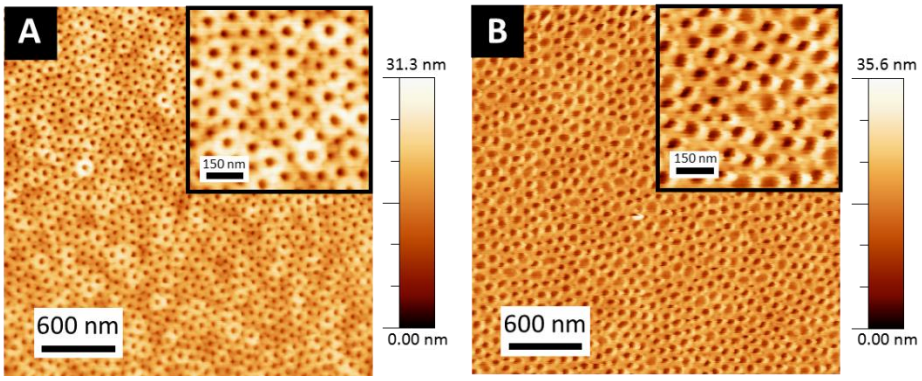

Figure 5: Topographical AFM micrographs of cylindrical PS-b-P4VP porous films with CH3COOH:P4VP ratios of A) 1:1, B) 10:1, obtained after a reconstruction in CH3COOH for 1h.

Indeed, porous obtained from the smaller micelles (1:1 CH_3COOH:P4VP ratio), present a diameter of 32±1.6 nm (Figure 5A), in contrast with the 48±2.1 nm diameter shown by the ones prepared from bigger micelles (10:1 CH_3COOH:P4VP ratio), as it is introduced in Fig 5B (See Fig S5 for more details about the pore size calculation). For comparison, when pristine BCP were immersed

on the pure CH_3COOH solution, cylindrical pores of 21±2.1 nm were obtaining.. This change of 11 nm and 27 nm respectively in the pore size, due to the presence of CH_3COOH molecules in the starting micellar films, shows the great potential of this approach to generate on-demand mesoporous structures.

Control of polymer morphology using different carboxylic acids.

In order to study also the influence of the SM size in the starting polymer film, several carboxylic acids were employed. Fig 6 shows the results obtained using formic acid (HCOOH), CH_3COOH and Propionic acid as SM respectively, in a 10:1 ratio SM:P4VP and a BCP concentration of 0.7 wt. % in all the cases. Different morphological transitions are clearly observed: from 90 nm diameter micelles obtained using HCOOH as SM (Fig 6B) to out-of-plane lamellae system when propionic acid is employed (Fig 6D). Out-of-plane cylinders are obtained in the case of using a solution with CH_3COOH as SM (Fig 6C).

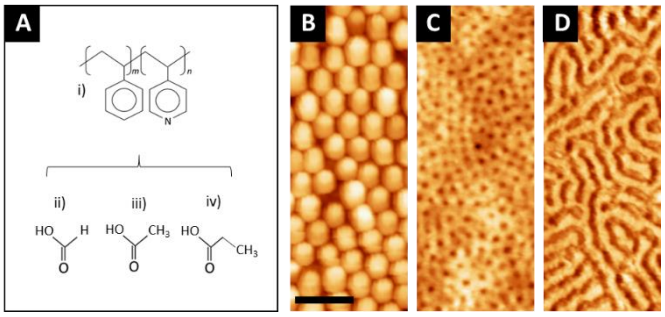

Figure 6: (A) Chemical structure of the small molecules used during this study and AFM topographical images of the various morphologies obtained by using different aliphatic carboxylic acids: A) micelles (HCOOH); B) out-of-plane cylinders (CH_3COOH) and C) lamellae (propionic acid). Scale bar represents 200 nm.

In all the cases the SM were linked to the P4VP domains by H-bonding. The morphological transitions, from micelles to cylinders or lamellae may be explained by the differences in the carboxylic chain length of the acids employed. Note that the presence of the SM modify the relative volume fractions of each block, shifting the BCP phase diagram and involving several order to order transition (OOT).

Conclusions

The production of surfaces with a controllable and tuneable porosity is a challenge for a broad range of BCP applications. During this work, the use of CH3COOH as a host molecule for PS-b-P4VP copolymer solutions was found to provide micellar films with different micelle size. A subsequent reconstruction process in ethanol, extracts the acetic acid H-bonded to the pyridine moiety, offering a mild and direct method to prepare nanoring porous films with controllable dimensions. The pore morphology may be tuned controlling the solvent used during the reconstruction process. Thereby cylindrical pores with dimensions ranging from 32 to 48 nm have been obtained using CH3COOH as solvent during the reconstruction process. Finally, the great potential and versatility of this approach have been shown with the employment of different carboxylic acid in order to tune the BCP morphology of the starting films.

Acknowledgements

Work supported by Spanish MINECO (grants FIS2013-45469 and FIS2016-76058 (AEI/FEDER,EU)). AAF wish to thank Dr. Stefan Guldin for his help during the preparation of the manuscript and the useful discussions.

References

1 J. Germain, J. Hradil, J. M. J. Fréchet and F. Svec, *Chem. Mater.*, 2006, **18**, 4430–4435.

2 P. Wang, M. Wang, F. Liu, S. Ding, X. Wang, G. Du, J. Liu, P. Apel, P. Kluth, C. Trautmann and Y. Wang, *Nat. Commun.*, 2018, **9**, 569.

3 F. M. Wisser, J. Grothe and S. Kaskel, *Sensors Actuators, B Chem.*, 2016, **223**, 166–171.

4 B. Reid, A. Taylor, Y. Chen, B. Schmidt-Hansberg and S. Guldin, *ACS Appl. Mater. Interfaces*, 2018, **10**, 10315–10321.

5 D. Wu, F. Xu, B. Sun, R. Fu, H. He and K. Matyjaszewski, *Chem. Rev.*, 2012, **112**, 3959–4015.

6 M. Zhou, Y. N. Wu, P. Luo, J. Lyu, D. Mu, A. Li, F. Li and G. Li, *RSC Adv.*, 2017, **7**, 49568–49575.

7 Y. Wang, *Acc. Chem. Res.*, 2016, **49**, 1401–1408.

8 T. A. Rebbecchi and Y. Chen, *J. Mater. Res.*, 2018, **33**, 2–15.

9 F. S. Bates and G. H. Fredrickson, *Annu. Rev. Phys. Chem.*, 1990, **41**, 525–557.

10 V. Castelletto and I. W. Hamley, *Curr. Opin. Solid State Mater. Sci.*, 2004, **8**, 426–438.

11 C. G. Gamys, J.-M. Schumers, C. Mugemana, C.-A. Fustin and J.-F. Gohy, *Macromol. Rapid Commun.*, 2013, **34**, 962–982.

12 D. A. Olson, L. Chen and M. A. Hillmyer, *Chem. Mater.*, 2008, 20, 869–890.

13 Y. Wang and F. Li, *Adv. Mater.*, 2011, **23**, 2134–2148.

14 H. Huang, B. Chung, J. Jung, H. W. Park and T. Chang, *Angew. Chemie - Int. Ed.*, 2009, **48**, 4594–4597.

15 H. Qiu, A. M. Oliver, J. Gwyther, J. Cai, R. L. Harniman, D. W. Hayward and I. Manners,

Macromolecules, 2019, **52**, 113–120.

16 J. Proust, J. Plain, T. Maurer, S. S. Lamarre, A. M. Ritcey, H. Yockell-Lelièvre and A. Sarrazin, *J. Nanoparticle Res.*, 2013, **15**, 1656.

17 L. Wang, F. Montagne, P. Hoffmann and R. Pugin, *Chem. Commun.*, 2009, **0**, 3798.

18 T. Lerond, J. Proust, H. Yockell-Lelièvre, D. Gérard and J. Plain, *Appl. Phys. Lett.*, 2011, **99**, 123110.

19 X. Zu, J. Gong, W. Tu and Y. Deng, *Macromol. Rapid Commun.*, 2011, **32**, 1526–1532.

20 A. C. Miller, R. D. Bennett, P. T. Hammond, D. J. Irvine and R. E. Cohen, *Macromolecules*, 2008, **41**, 1739–1744.

21 Z. Chen, C. He, F. Li, L. Tong, X. Liao and Y. Wang, *Langmuir*, 2010, **26**, 8869–8874.

22 K. Evans and T. Xu, *Macromolecules*, 2019, **52**, 639–648.

23 B. K. Kuila and M. Stamm, *J. Mater. Chem.*, 2011, **21**, 14127–14134.

24 G. P. Wu, X. Liu, X. Chen, H. S. Suh, X. Li, J. Ren, C. G. Arges, F. Li, Z. Jiang and P. F. Nealey, *Adv. Mater. Interfaces*, 2016, **3**, 1600048.

25 B. K. Kuila, M. S. Rama and M. Stamm, *Adv. Mater.*, 2011, **23**, 1797–1800.

26 S. Roland, D. Gaspard, R. E. Prud'Homme and C. G. Bazuin, *Macromolecules*, 2012, **45**, 5463–5476.

27 D. Chen and M. Jiang, *Acc. Chem. Res.*, 2005, **38**, 494–502.

28 A. Álvarez-Fernández, F. Valdés-Bango, R. Losada-Ambrinos, J. I. Martín, M. Vélez, J. M. Alameda and F. J. García Alonso, *Polym. Int.*, 2018, **67**, 393–398.

29 X. Zu, J. Gong, W. Tu and Y. Deng, *Macromol. Rapid Commun.*, 2011, **32**, 1526–1532.

30 M. F. Schulz, A. K. Khandpur, F. S. Bates, K. Almdal, K. Mortensen, D. A. Hajduk and S.

M. Gruner, *Macromolecules*, 1996, **29**, 2857–2867.

31 W. Zha, C. D. Han, D. H. Lee, S. H. Han, J. K. Kim, J. H. Kang and C. Park, *Macromolecules*, 2007, **40**, 2109–2119.

32 I. Horcas, R. Fernández, J. M. Gómez-Rodríguez, J. Colchero, J. Gómez-Herrero and A. M. Baro, *Rev. Sci. Instrum.*, 2007, **78**, 013705.

33 M. Borsboom, W. Bras, I. Cerjak, D. Detollenaere, D. Glastra Van Loon, P. Goedtkindt, M. Konijnenburg, P. Lassing, Y. K. Levine, B. Munneke, M. Oversluizen, R. Van Tol and E. Vlieg, *J. Synchrotron Radiat.*, 1998, **5**, 518–520.

34 G. Portale, D. Cavallo, G. C. Alfonso, D. Hermida-Merino, M. Van Drongelen, L. Balzano, G. W. M. Peters, J. G. P. Goossens and W. Bras, *J. Appl. Crystallogr.*, 2013, **46**, 1681–1689.

35 W. Bras, I. P. Dolbnya, D. Detollenaere, R. Van Tol, M. Malfois, G. N. Greaves, A. J. Ryan and E. Heeley, in *Journal of Applied Crystallography*, 2003, vol. 36, pp. 791–794.

36 S. H. Yun, S. Il Yoo, J. C. Jung, W. C. Zin and B. H. Sohn, *Chem. Mater.*, 2006, **18**, 5646–5648.

37 D. Chen and M. Jiang, *Acc. Chem. Res.*, 2005, **38**, 494–502.

38 B. K. Kuila and M. Stamm, *J. Mater. Chem.*, 2011, **21**, 14127–14134.

39 P. Madhavan, K. V. Peinemann and S. P. Nunes, *ACS Appl. Mater. Interfaces*, 2013, **5**, 7152–7159.

40 S. Roland, C. Pellerin, C. G. Bazuin and R. E. Prudhomme, *Macromolecules*, 2012, **45**, 7964–7972.

41 S. Jiang, A. Göpfert and V. Abetz, *Macromolecules*, 2003, **36**, 6171–6177.

42 N. V. Drichko, G. Y. Kerenskaia and V. M. Schreiber, *J. Mol. Struct.*, 1999, **477**, 127–141.

43 M. Tiitu, M. Torkkeli, R. Serimaa, T. Mäkelä and O. T. Ikkala, *Solid State Ionics*, 2005,

176, 1291–1299.

44 X. Ye, B. J. Edwards and B. Khomami, *Macromol. Rapid Commun.*, 2012, **33**, 392–395.

45 L. Wang, F. Montagne, P. Hoffmann and R. Pugin, *Chem. Commun.*, 2009, **0**, 3798.

46 M. Aizawa and J. M. Buriak, *Chem. Mater.*, 2007, **19**, 5090–5101.

47 J. Wernecke, H. Okuda, H. Ogawa, F. Siewert and M. Krumrey, *Macromolecules*, 2014, **47**, 5719–5727.

48 M. K. Endoh, M. Stamm, E. B. Gowd, T. Koga and K. Kumar, *Soft Matter*, 2014, **10**, 7753–7761.

49 Tiberio A. Ezquerra, *Applications of Synchrotron Light to Non-Crystalline Diffraction in Materials and Life Science*, Springer, 2006.